



HAL
open science

Measuring enhanced optical correlations induced by transmission open channels in a slab geometry

N Verrier, L Depreter, D Felbacq, M Gross

► **To cite this version:**

N Verrier, L Depreter, D Felbacq, M Gross. Measuring enhanced optical correlations induced by transmission open channels in a slab geometry. 2015. hal-01181347v1

HAL Id: hal-01181347

<https://hal.science/hal-01181347v1>

Preprint submitted on 30 Jul 2015 (v1), last revised 31 Jul 2015 (v2)

HAL is a multi-disciplinary open access archive for the deposit and dissemination of scientific research documents, whether they are published or not. The documents may come from teaching and research institutions in France or abroad, or from public or private research centers.

L'archive ouverte pluridisciplinaire **HAL**, est destinée au dépôt et à la diffusion de documents scientifiques de niveau recherche, publiés ou non, émanant des établissements d'enseignement et de recherche français ou étrangers, des laboratoires publics ou privés.

Measuring enhanced optical correlations induced by transmission open channels in a slab geometry

N. Verrier,¹ L. Depreter,¹ D. Felbacq,¹ and M. Gross¹

¹Laboratoire Charles Coulomb - UMR 5221 CNRS-UM Université
Montpellier Bat 11. Place Eugène Bataillon 34095 Montpellier

(ΩDated: July 30, 2015)

Light can be transmitted through disordered media with high efficiency due to the existence of open channels, but quantitative agreement with theory is difficult to obtain because of the large number of channels to control. By measuring, by digital holography, the correlations of the transmitted field, we are able to determine the number of channels involved in transmission. With sample, the number of channels is divided by about 15 with respect to what is expected without sample. This figure is in good agreement with the theoretical prediction.

PACS numbers: 42.25.Bs Wave propagation, transmission and absorption; 05.60.Cd Classical transport; 02.10.Yn Matrix theory; 42.40.Ht Hologram recording and readout methods.

Wave propagation in complex media gives rise to a multitude of effects that physicists are trying to understand and analyze both experimentally and theoretically. Some of these effects, such as coherent backscattering were observed [1, 2], and are well understood. Others, like the 3D Anderson localization of an electromagnetic wave, are a kind of Holy Grail [3] that may exist or not. Other, are under study. For example, recent wavefront shaping and phase recording technologies make possible to focus and image through strongly scattering media [4–7], or to get enhanced transmission by adjusting the input mode structure to fit with the so-called "open channels" [8–10]. In the best case, the transmission was increased by a factor of 4 with respect to that observed without adjustment [8], while optimal transmission remains small as compared to the 100 % expected with open channels [11].

Two methods have been used to study this open channel effect. The first method is to change the mode structure of the incident field with a spatial light modulator (SLM) to maximize the transmission [10]. Once the maximum is reached, it is considered that the incident mode fits with an open channel, and that the obtained transmission is that of an open channel (ideally 100%). The second method is to measure and to diagonalize the transmission matrix \mathbf{t} [7]. The eigenvectors, whose eigenvalues are maximal, correspond to open channels [8, 9].

The study of open channels in an open geometry (slab) by both methods presents great difficulties because of the large number N_g of geometrical modes (or channels) to control or measure. Indeed, the observation of significant effects requires a medium, whose thickness l is large compared to the light transport mean free path l^* . Furthermore, lateral dimensions L should be large compared with the thickness l so that the effect can be analyzed easily. So we must have $L \gg l \gg l^*$, i.e. for example $l \sim 10l^*$ and $L \sim 100l^*$. On the other hand, it holds $N_g = 2\pi S/\lambda^2$ (for 2 polarisations), where $S = L^2$ is the sample area, and λ the wavelength. Since $l^* \sim \lambda$ in the best case, we get $N_g \sim 10^5$. This number is much higher

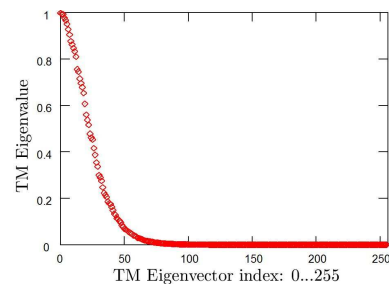


FIG. 1: Typical distribution of the eigenvalues t_n of $\mathbf{t} \mathbf{t}^\dagger$ plotted in decreasing order. Eigenvectors are calculated by using a typical transmission matrix $[\mathbf{t}]$ of size $N \times N$ with $N = 256$ obtained by Monte Carlo. The parameters of the calculation are adjusted to get an average transmission $\sum_{n=1}^{256} t_n^2 \simeq 0.1$.

than the number of modes controlled or measured in experiments [9, 10].

Popoff et al. [10] control only 650 modes. They get an increase in the transmission by a factor 3, but nothing indicates that the optimization process is completed, and that the obtained maximum of transmission corresponds to an open channel. Yu et al. [9] perform measurements on a base of 21078 modes, and the distribution of the eigenvalues they get is quite far from that predicted by the open channel theory.

Rather than preparing open channels which is a difficult task, we propose to study the outgoing field, which is directly observable. This field is distributed over a number N_2 of modes, which is about the number of open channels, that is $N_g l^*/l$ [12], this is thus much smaller than the number of geometrical modes N_g . For random incoming fields, one expects thus to observe larger correlations for the outgoing field than for the incoming one. In the following it is shown that these correlations can indeed be used to define and measure N_2 , that they provide a mean to highlight the open channel effect by measuring the ratio $N_g/N_2 \gg 1$, and to make quantitative compar-

ison with theory.

To be more specific, let us consider the eigenvectors \mathbf{U}_n of $\mathbf{t}^\dagger \mathbf{t}$ where \mathbf{t} is the transmission matrix. These eigenvectors \mathbf{U}_n , whose eigenvalues are t_n^2 (where $t_n > 0$ is real) constitute a natural orthonormal basis of the incoming field \mathbf{E}_1 with $\mathbf{U}_n \cdot \mathbf{U}_{n'} = \delta(n, n')$. Similarly, the eigenvectors \mathbf{V}_n of $\mathbf{t} \mathbf{t}^\dagger$ constitute an orthonormal basis of the outgoing field \mathbf{E}_2 with $\mathbf{V}_n \cdot \mathbf{V}_{n'} = \delta(n, n')$. \mathbf{U}_n and \mathbf{V}_n are related together by $\mathbf{t} \mathbf{U}_n = t_n \mathbf{V}_n$. We calculated, by Monte Carlo, a typical transmission matrix \mathbf{t} obtained for $N_g = 256$ modes in the random matrix theory ideal case, and we calculated the eigenvector \mathbf{U}_n and the eigenvalue t_n^2 . Like Choi et al. [13], we have plotted on Fig.1 the eigenvalues t_n^2 in decreasing order from $t_n^2 = 1$ for $n = 1$ down to $t_n^2 \simeq 0$ for $n = 256$. The calculation was made for $l = 9l^*$ to get an average transmission for energy $T = (1/N) \sum_{n=1}^N t_n^2$ close to 0.1. The open channels correspond here to the first eigenvectors, with $t_n^2 \simeq 1$, while the outgoing channels correspond to the channels, whose transmission t_n^2 is noticeable ($n = 1$ to about 40). \mathbf{E}_1 is distributed over all modes \mathbf{U}_n with $n = 1$ to 256, while the outgoing field \mathbf{E}_2 is mainly distributed over the so-called "outgoing modes" \mathbf{V}_n with $n = 1$ to about 40.

Let us consider a typical input field $\mathbf{E}_1 = \sum_{n=1}^{N_g} c_n \mathbf{U}_n$, where c_n are independent identically distributed Gaussian complex random numbers. The outgoing field is $\mathbf{E}_2 = \mathbf{t} \mathbf{E}_1 = \sum_{n=1}^{N_g} c_n t_n \mathbf{V}_n$. The incoming and outgoing energies are respectively $|\mathbf{E}_1|^2 = \sum_{n=1}^{N_g} |c_n|^2$ and $|\mathbf{E}_2|^2 = \sum_{n=1}^{N_g} t_n^2 |c_n|^2$. The Monte Carlo calculation gives a transmission efficiency $|\mathbf{E}_2|^2/|\mathbf{E}_1|^2$ close to $T = 0.1$. If \mathbf{E}_2 is re-injected into the sample by using a phase conjugation mirror, we get the twice transmitted field (i.e. the outgoing field that is back transmitted through the sample) $\mathbf{E}_3 = \sum_{n=1}^{N_g} c_n t_n^2 \mathbf{U}_n$, whose energy is $|\mathbf{E}_3|^2 = \sum_{n=1}^{N_g} t_n^4 |c_n|^2$. We can define the back transmission T_B of the outgoing field by $T_B = |\mathbf{E}_3|^2/|\mathbf{E}_2|^2$. We got $T_B = 2/3$ as expected [5, 11].

In this letter, we propose to study the "equivalent numbers of modes" N_1 and N_2 of the incoming (\mathbf{E}_1) and outgoing field (\mathbf{E}_2). Since \mathbf{E}_1 is uniformly distributed over all the N_g geometrical modes \mathbf{U}_n , one has $N_1 = N_g$. On the other hand, it holds $N_2 \ll N_g$ since \mathbf{E}_2 is distributed over a much smaller number of outgoing modes \mathbf{V}_n . The "equivalent number of modes" N_2 corresponds here to the "width" of the curve t_n^2 (i.e. $N_2 \simeq 40$ for the example plotted on Fig.1).

In order to define N_2 more precisely, we considered two uncorrelated random incoming fields $\mathbf{E}_1 = \sum_{n=1}^{N_g} c_n \mathbf{U}_n$ and $\mathbf{E}'_1 = \sum_{n=1}^{N_g} c'_n \mathbf{U}_n$ having the same energy $|\mathbf{E}_1|^2 = |\mathbf{E}'_1|^2$, and the corresponding outgoing fields $\mathbf{E}_2 = \sum_{n=1}^{N_g} c_n t_n \mathbf{V}_n$ and $\mathbf{E}'_2 = \sum_{n=1}^{N_g} c'_n t_n \mathbf{V}_n$. One can then calculate the normalized residual correlation C_1 and C_2

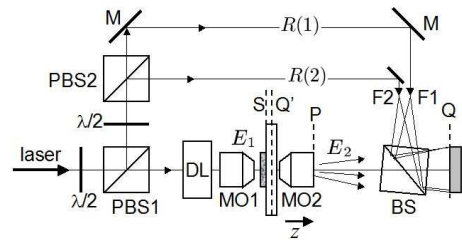


FIG. 2: Experimental setup. E_1 : incoming field; E_2 : outgoing field; $R(1)$, $R(2)$: reference fields of polarisation $p=1$ and $p=2$; PBS1, PBS2: polarized beam splitters; $\lambda/2$: half wave plate to control E_1 , $R(1)$ and $R(2)$ respective power; BS: beam splitter; M: mirror; DL: diffusing liquid; MO1 and MO2: microscope objectives; Q, Q': camera plane, and camera conjugate plane with respect to MO2; S: sample outgoing plane.

for the incoming and outgoing fields.

$$C_1 = \frac{\mathbf{E}_1 \cdot \mathbf{E}'_1}{|\mathbf{E}_1|^2} = \frac{\sum_{n=1}^{N_g} c_n c'_n}{\sum_{n=1}^{N_g} |c_n|^2} \quad (1)$$

$$C_2 = \frac{\mathbf{E}_2 \cdot \mathbf{E}'_2}{|\mathbf{E}_2|^2} = \frac{\sum_{n=1}^{N_g} c_n c'_n t_n^2}{\sum_{n=1}^{N_g} |c_n|^2 t_n^2}$$

We calculated the statistical averages $\langle |C_1|^2 \rangle$ by Monte Carlo and got $\langle |C_1|^2 \rangle = 1/N_g = 1/N_1$. This result can be proved rigorously (see the supplementary material). This suggest to define the equivalent number of mode N_2 by $\langle |C_2|^2 \rangle = 1/N_2$. We have then calculated typical transmission matrices \mathbf{t} for $N_g = 256, 512$ and 1024 and for $l/l^* = 1$ to 40. For each \mathbf{t} we have calculated $\langle |C_2|^2 \rangle$ (and thus N_2) by Monte Carlo. For $l/l^* \gg 1$, we got the simple empirical formula:

$$N_2 = (3/2) T N_g \quad (2)$$

The number of outgoing mode N_2 is thus $3/2 \times$ larger than number of open channels ($T N_g$).

The key idea of this work is that $\langle |C_2|^2 \rangle$ and N_2 can be easily measured experimentally, with a time varying random incoming field, which is uncorrelated at times t and t' . Indeed, one can get the correlation C_2 from the measured outgoing field $E_2(x, y, t, p)$ (where x, y are the transverse coordinates, t the time, and $p = 1, 2$ the polarisation) by:

$$C_2(t, t') = \frac{\sum_{x,y,p} E_2(x, y, t, p) E_2^*(x, y, t', p)}{\sum_{x,y,p} |E_2(x, y, t, p)|^2} \quad (3)$$

The importance of open channels can be directly demonstrated by measuring $N_2 = 1/\langle |C_2|^2 \rangle$ and by verifying that $N_2/N_g \ll 1$. Furthermore, a quantitative comparison with our empirical model can be made by verifying Eq.2 experimentally.

Figure 2 shows the setup we used to study the open channels by measuring $E_2(x, y, t, p)$ and by calculating C_2 by Eq.3. The setup consists of a Mach-Zehnder off-axis interferometer with two orthogonally polarized reference beams. The light emitted by a $\lambda = 532$ nm, 70 mW laser is split into a reference and an object field using a polarizing beam splitter (PBS1). The studied sample is a ZnO powder slab with thickness $l = 22 \mu\text{m} \pm 7 \mu\text{m}$ deposited on a microscope cover slide. In order to maximize the collection of both input and output modes, the sample is positioned between two microscope objectives: MO1 (NA = 0.9 air, x60) in the powder side, and MO2 (NA = 1.4 oil, x60) in the cover slide side.

A tank (1.5 cm thick) filled with viscous diffusing liquid (glycerol + concentrated milk) is positioned in front of MO1 to randomize the illumination structure in both time and space. The incoming field E_1 is therefore randomly distributed over all the incoming modes and varies in time. Thus, considering $|t - t'| > 100$ ms, the fields $E_1(t)$ and $E_1(t')$ are uncorrelated.

Measurement of the outgoing field E_2 is holographically performed. The two orthogonally polarized reference beams $R(p)$ (where $p = 1, 2$ is polarization) interfere with the outgoing fields $E_2(p)$, and the interference pattern $I = \sum_{p=1,2} |R(p) + E_2(p)|^2$ is recorded on the CCD sensor (10 Hz, 1340×1040 pixels with $\Delta x = 6.45 \mu\text{m}$ pitch). This configuration makes it possible to calculate from I the complex amplitudes $E_2(p)$ of the outgoing fields along both polarizations $p = 1, 2$ directions by filtering, in the Fourier space, the desired +1 grating order i.e. $E_2(p)R^*(p)$ [14].

The Fourier spacial filtering is illustrated by Fig. 3. The 1340×1040 holograms were cropped to 1024×1024 (the imaged area is therefore $L = 77 \mu\text{m}$) and two frames holograms H were calculated from successive frames: $H(t_{2n}) = I(t_{2n}) - I(t_{2n+1})$. The Fourier hologram $\tilde{H}(k_x, k_y) = \text{FFT}[H(x, y)]$ (where FFT is the Fast Fourier transform) is then calculated. $|\tilde{H}|^2$ is displayed on Fig. 3(a). Four bright circular regions can be observed. They correspond to the +1 grating order $E_2(p)R^*(p)$ for $p = 1$ (zone 1), and $p = 2$ (zone 2), and to the -1 grating order $E_2^*(p)R(p)$ for $p = 2$ (zone 3) and $p = 1$ (zone 4). Because the calculations are made with two frames hologram, the zero order terms $|R(p)|^2$ cancel, and are not visible on Fig. 3(a).

Note that the angular tilt of the beam splitter BS as well as the source point positions F_1 and F_2 (see Fig. 2) have been chosen so that the four regions in Fig. 3(a) do not overlap, and have sharp edges. From Fig. 3(a), we have selected the desired +1 grating orders E_2R^* by cropping zone 1 and zone 2 (for $p = 1$ and 2) and by taking the inverse Fourier transform of the cropped zones: $E_2R^*(x, y, p) = \text{FFT}^{-1}C_p[\tilde{H}(k_x, k_y, p)]$, where C_p is the crop operator for polarisation p .

Since $R(p)$ is roughly constant with the position x, y ,

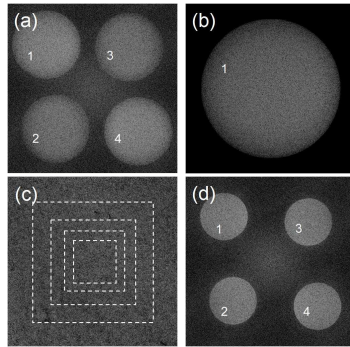


FIG. 3: $|\tilde{H}|^2$ (a,d); $|\tilde{H}_1|^2$ zoomed $\times 2$ (b); $|H_1|^2$ (c). In (c), the dashed squares of size $M = 724, 512, 362$ and 256 pixels illustrate the ability to select different zones of the sample to calculate $\langle |C_2|^2 \rangle$. Images are obtained with ZnO sample (a-c), and without (d).

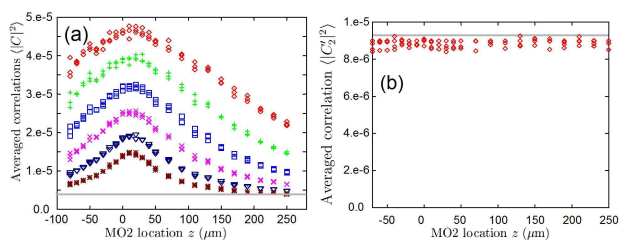


FIG. 4: (a) Averaged correlation $\langle |C|^2 \rangle$ measured with ZnO plotted as function of MO2 position z . Calculation is made with $M \times M$ pixels with $M = 1024$ (red diamonds), 362 (green crosses), 256 (blue rectangles), 181 (purple crosses), 128 (dark blue triangles) and 90 (brown stars). Solid grey lines is $1/N_g = 3.83e-6$. (b) Averaged correlation $\langle |C'|^2 \rangle$ measured without ZnO. Solid grey line is $1/N'_g = 9.286e-6$.

the correlations $C_2(t, t')$ can be then calculated by replacing $E_2(x, y, p, t)$ by $[E_2R^*](x, y, p, t)$ in Eq. 1. The statistical average $\langle |C_2|^2 \rangle$ was obtained by first recording the sequences of 150 camera frames: $I(t_0) \dots I(t_{149})$, at times: $t_n = n\Delta t$ and $\Delta t = 100$ ms, yielding 75 hologram: $H(t_0), H(t_2) \dots H(t_{148})$, which were used to calculate $[E_2R^*](x, y, p, t_{2n})$ and $C_2(t_{2n}, t_{2n'})$, and then by averaging $|C_2(t_{2n}, t_{2n'})|^2$ for all couple of times $t_{2n}, t_{2n'}$ with $|n - n'| > 5$ and $n, n' = 0..74$. Because of experimental defects, $|R(p)|$ varies slightly with position. This affects the calculation of $C_2(t, t')$ and $\langle |C_2|^2 \rangle$. In order to account for this effect, we measured $|R(x, y, p)|$ from our stack of holographic data and we calculated $C_2(t, t')$ with $[E_2R^*](x, y, p, t)/|R(x, y, p)|$. This correction is about 10% for $\langle |C_2|^2 \rangle$.

It should be noted that the experimental tradeoffs (i.e. diffusing liquid randomized illumination instead of SLM, two frame holograms ...) were made in order to minimize the correlation bias within the incoming fields E_1 . In particular, two frames holograms minimize bias due to ballistic light that travel through the diffusing tank.

To have an extra control parameter, the MO2 position along z can be adjusted by a motorized micrometer device. For $z \simeq 0$, the camera's conjugated plane Q' coincides with the exit plane S of the sample, and the plane S is on focus on the camera. This configuration maximizes the open channel effect. When $|z| \neq 0$ increases, the measurement plane Q' no longer coincides with S and $\langle |C_2|^2 \rangle$ decreases. Indeed, if Q' \neq S, the correlation C_2 is calculated without being able to define precisely the sample selected zone where the outgoing field is measured: points outside of the zone contribute to the signal, and points inside the zone contribute less since the detection angle is lower [17]. Controlling z provides thus an experimental mean to decrease and even to suppress the open channel effect. This is expected to occur when z becomes much larger than the sample transverse size L . In that case, $\langle |C_2|^2 \rangle$ must be close to $\langle |C_1|^2 \rangle = 1/N_g$.

Data are acquired by moving MO2 from $z=Q'S=-80$ to $250 \mu\text{m}$ by step $\Delta z=10$ or $20 \mu\text{m}$. For each position of MO2, a sequence of 150 frames is recorded. $\langle |C_2|^2 \rangle$ is then calculated for different transverse size $L = M\Delta x$ of the selected zone. This is made by cropping the data over x , and y . The cropped zones are represented by the dotted squares in Fig.3 (c). In order to better compare the results obtained with different M , $\langle |C_2|^2 \rangle$ is multiplied by $M^2/1024^2$ to compensate for area variation. This factor is equal to 1 for $M = 1024$ (i.e. $L = 77 \mu\text{m}$). This provides a second experimental mean to decrease the effect of open channels when the transverse size L of the sample becomes smaller than its thickness l , since, in that case, the transverse geometrical losses becomes large. Conversely, by extrapolating L toward infinite, one can get an estimate of the maximum enhancement of correlation that is expected for a given thickness l of the sample.

We have verified experimentally that changing z and M does not modify the detected energy per unit of area. We have plotted on Fig. 4 (a) $M^2\langle |C_2|^2 \rangle/1024^2$ as a function of the MO2 position z for $M = 1024$ (red diamonds), 362 (green crosses), 256 (bleue rectangles), 181 (purple crosses), 128 (dark blue triangles) and 90 (brown stars). As expected $\langle |C_2|^2 \rangle$ is maximum for $z \simeq 0$, and decreases with $|z|$. When the sample size M decreases, the geometrical losses increase, and $M^2\langle |C_2|^2 \rangle/1024^2$ decreases too. Moreover, the peak of correlation becomes narrower, and the correlation reaches a plateau for small M and large z (e.g. $M = 90$ and $z = 250 \mu\text{m}$). This plateau is reached when geometrical losses are large, that is when $z \gg l, L$.

We compared this plateau with the correlation $\langle |C_1|^2 \rangle = 1/N_g$ that is expected without open channels. The usual relation that defines the number of geometrical mode N_g should be corrected to account for the refractive index n of the medium where the output field is collected (factor $\times n^2$), and for the detection solid angle (factor $\times [\text{NA}]^2/n^2$) where NA is the numerical aperture

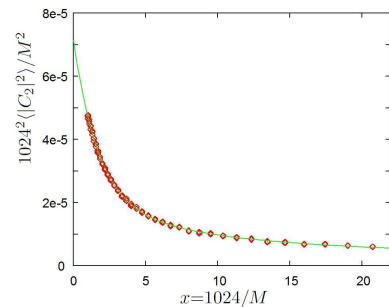


FIG. 5: Maximum averaged correlation $1024^2\langle |C_2|^2 \rangle/M^2$ according to $x = 1024/M$. Measured point are red diamonds. Solid green line is $a_1e^{-x/b_1} + a_2e^{-x/b_2} + a_3$, with $a_1=5.19\text{e-}5$, $a_2=1.59\text{e-}5$, $b_1=1.7$, $b_2=10.0$ and $a_3=3.67\text{e-}6 \simeq 1/N_g$.

of the detection objective. One gets thus:

$$N_g = 2\pi[\text{NA}]^2 L^2 / \lambda^2 \quad (4)$$

where L is the transverse size of the sample and λ the wavelength in vacuum. For $\text{NA}=1.4$ and $L=77 \mu\text{m}$, we get $1/N_g=3.83\text{e-}6$ (solid grey line on Fig.4(a)) in good agreement with the plateau of correlation curves $M^2\langle |C_2|^2 \rangle/1024^2$. This agreement validates our correlation-based theoretical approach and proves that we have correctly evaluated the number of geometrical modes by Eq.4 .

We conducted a control experiment without ZnO sample and we calculated the correlation $\langle |C_2'|^2 \rangle$ versus z for $M = 1024$. As seen on Fig.4 (b), $\langle |C_2'|^2 \rangle$ is much lower than with the sample, and does not depend on z position. Moreover, $\langle |C_2'|^2 \rangle \simeq 8.8\text{e-}6$ is close to the correlation that is expected without open channels $\langle |C_1'|^2 \rangle = 1/N_g' = 9.3\text{e-}6$ (see solid grey line on Fig.4(b)). Note here that the number of geometrical mode N_g' must be calculated by Eq.4 with MO1 numerical aperture (i.e. $\text{NA}=0.9$). Indeed, the signal collection angle is limited by MO1. This point is illustrated by Fig.3 (d) that displays the hologram $|\tilde{H}|^2$ we got without sample. $|\tilde{H}|^2$ exhibits four bright circular zones that are smaller in diameter than with the sample (Fig.3(a)). These circles correspond to the MO1 pupil located in the plane P' that appears sharp in the plane P, because MO1 and MO2 form an afocal optical system.

To calculate the correlation that is expected without lateral geometrical losses of you slab sample, we have plotted on Fig. 5 (red diamonds), the maximum of $M^2\langle |C_2|^2 \rangle/1024^2$ obtained during the z scan, as a function of $x = 1024/M$. We extrapolated our results to $L = \infty$ by fitting the data with a sum of 2 decreasing exponentials (see solid green line on Fig.5). Extrapolation to $L=\infty$ (i.e. $x = 0$) yields $M^2\langle |C_2|^2 \rangle/1024^2=7.15\text{e-}5$. Half maximum is reached for $x=1.73$ i.e. $L=50 \mu\text{m}$ (about twice the thickness l). The importance of open channels that corresponds to $N_g/N_2 \gg 1$ is here clearly demonstrated, since we got $N_g/N_2=12.3$ without extrap-

olation for $L = 77 \mu\text{m}$, and 18.6 after extrapolation to $L = \infty$.

The N_g/N_2 measured ratio must *a priori* be corrected by the collection angle of the objectives MO1 and MO2 [15]. MO2 losses yield a geometrical loss factor $[\text{NA}]^2/n^2=0.85$ that affects N_g (see Eq.4). Monte Carlo calculations [18] show that they affect N_2 by roughly the same amount when $N_g/N_2 \gg 1$. The ratio N_g/N_2 is thus not modified by the MO2 losses. On the other hand, the MO1 losses decrease the number of incoming geometrical modes $N_1 = N'_g$ by a factor $0.9^2/1.52^2=0.35$. This factor was accounted for to get the $1/N'_g$ solid grey line displayed on Fig.4 (b). Calculations show that this decrease of N_1 by 0.35 yields a small decrease of N_2 ($\simeq 0.9$) as noticed by Kim et al. [16]. The corrected extrapolated ratio is thus $N_g/N_2=16.74$.

To perform a quantitative comparison of our results with Eq.2 empirical formula, we measured the transmission T . The ratio of the signal energy ($\sum |E_2|^2$) detected with and without sample is $1/30 \pm 20 \%$ [19]. Taking into account the MO2 losses ($\times 0.85$) [20], we get $T = (1/30)/0.85 \simeq 1/25$. The ratio that is expected from Eq.2 is thus $N_g/N_2=2/3T=16.6 \pm 20 \%$, in good agreement with the corrected extrapolated experimental results 16.74. Although this agreement is already extremely encouraging, the proposed approach can still be improved to provide better quantitative results. A more precise measurement of the sample thickness l , and average transmission T should be made. A setup using a high NA oil objective for MO1 yielding roughly the same number of geometrical modes for input and output (i.e. $N_g \simeq N'_g$) would also give a better highlight of the open channel effect.

More fundamentally, the shapes of Fig.4 (a) network curves, and of Fig.5 curve give informations that were exploited not. Indeed, these curves characterize the dependence of $\langle |C^2| \rangle$ with the MO2 defocus z , the sample transverse size L and the sample thickness l , i.e. with the slab geometry. In order to exploit these informations a theory that accounts for the slab geometry should be developed. We hope that the present results will encourage such development. We acknowledge ANR-2011-BS04-017-04 grant for funding.

[1] M.P. Van Albada and A. Lagendijk. Observation of weak localization of light in a random medium. *Phys. Rev. Lett.*, **55**, 2692 (1985).

[2] P.E. Wolf and G. Maret. Weak localization and coherent

backscattering of photons in disordered media. *Phys. Rev. Lett.* **55**, 2696, (1985).

- [3] Philip W Anderson. Absence of diffusion in certain random lattices. *Phys. Rev.* **109**, 1492 (1958).
- [4] I.M. Vellekoop and A.P. Mosk. Focusing coherent light through opaque strongly scattering media. *Opt. Lett.* **32** 2309 (2007).
- [5] IM Vellekoop and AP Mosk. Universal optimal transmission of light through disordered materials. *Phys. Rev. Lett.* **101** 120601 (2008).
- [6] I.M. Vellekoop, A. Lagendijk, and A.P.Mosk. Exploiting disorder for perfect focusing. *Nature Photon.* **4** 320 (2010).
- [7] S.M. Popoff, G. Lerosey, R. Carminati, M.Fink, A.C. Boccara, and S. Gigan. Measuring the transmission matrix in optics: an approach to the study and control of light propagation in disordered media. *Phys. Rev. Lett.* **104** 100601 (2010).
- [8] M. Kim, Y. Choi, C. Yoon, W. Choi, J. Kim, Q.H. Park, and W. Choi. Maximal energy transport through disordered media with the implementation of transmission eigenchannels. *Nature Photon.*, **6** 581 (2012).
- [9] H. Yu, T.R. Hillman, W. Choi, J.O. Lee, M.S. Feld, R.R. Dasari, and Y. Park. Measuring large optical transmission matrices of disordered media. *Phys. Rev. Lett.* **111** 153902 (2013).
- [10] S.M. Popoff, A. Goetschy, S.F. Liew, A.D. Stone, and H. Cao. Coherent control of total transmission of light through disordered media. *Phys. Rev. Lett.* **112** 133903 (2014).
- [11] Y.V. Nazarov. Limits of universality in disordered conductors. *Phys. Rev. Lett.* **73** 134 (1994).
- [12] J.B. Pendry, A. MacKinnon, and P.J. Roberts. Universality classes and fluctuations in disordered systems. In *Proc. Roy. Soc. A* **437**, 67 (1992).
- [13] W. Choi, A.P. Mosk, Q.H. Park, and W. Choi. Transmission eigenchannels in a disordered medium. *Phys. Rev. B* **83** 134207 (2011).
- [14] E. Cuche, P. Marquet, and C. Depeursinge. Spatial filtering for zero-order and twin-image elimination in digital off-axis holography. *Appl. Opt.* **39** 4070 (2000).
- [15] A. Goetschy and A.D. Stone. Filtering random matrices: the effect of incomplete channel control in multiple scattering. *Phys. Rev. Lett.*, **111** 063901 (2013).
- [16] M.Kim, W. Choi, C. Yoon, G.H. Kim, and W. Choi. Relation between transmission eigenchannels and single-channel optimizing modes in a disordered medium. *Opt. Lett.*, **38** 2994 (2013).
- [17] The angle effect was calculated by Goetchy et al. [15]
- [18] similar to the ones made to get Eq. 2
- [19] This measurement can be affected by experimental drifts since the energy measurements made with and without sample are made at different days.
- [20] Without sample, all the light collected by MO1 is collected by MO2. With sample, 15% of the outgoing light is scattered out of the MO2 collecting angle.